Journal of Molecular Modeling (2020) 26: 89
https://doi.org/10.1007/s00894-020-04363-y

ORIGINAL PAPER

First-principles microkinetic analysis of dehydrogenation of cyclohexene on the Pt/Cu/Pt (111) surface

Shou Chun Feng [1] · Hong Yan Ma [1] · Peng Peng Hao [1]

Received: 25 January 2020 / Accepted: 23 March 2020 / Published online: 1 April 2020

Abstract

Three kinds of Pt-Cu bimetallic catalysts (Cu/Pt (111), Pt/Cu/Pt (111), and Pt_4Cu_5/Pt (111)) have been researched employing density functional theory (DFT) calculation, using dehydrogenation of cyclohexene to benzene as a probe reaction. The adsorption energies are basically in the sequence: Pt_4Cu_5/Pt (111) > Cu/Pt (111) ≈ Pt/Cu/Pt (111). The key step is $C_6H_9 \rightarrow C_6H_8$ on Cu/Pt (111) (0.85 eV) and Pt/Cu/Pt (111) (0.87 eV). On Pt_4Cu_5/Pt (111), the key step is $C_6H_7 \rightarrow C_6H_6$ (1.17 eV). The selectivity for gas phase benzene is in the order of Cu/Pt(111) > Pt/Cu/Pt(111) > Pt_4Cu_5/Pt(111), according to the energy difference between the barrier of benzene dehydrogenated to phenyl and benzene desorption. The co-adsorbed hydrogen atoms lead to improved selectivity for gas phase benzene on Cu/Pt (111) and Pt/Cu/Pt (111), by making benzene desorption easy but dehydrogenation difficult. However, the barrier of benzene dehydrogenation decreases with the increase of H coverage on the Pt_4Cu_5/Pt (111) due to obvious destabilized benzene, and thus the effect on Pt_4Cu_5/Pt (111) is closely related to the concentration of surface H. Attributed to thermodynamic stability, high activity, and selectivity for gas benzene, the Pt/Cu/Pt (111) structure is suggested as reasonable dehydrogenation catalyst, and the dehydrogenation process on Pt/Cu/Pt(111) has been further studied by microkinetic modeling. A volcano-like relationship is found between the adsorption of cyclohexene and the TOF (turnover frequency) of gas phase benzene. Secondly, two apparent activation energies are obtained: 0.77 eV (250~350 K) and 0.45 eV (350~650 K), implying the RDS (rate-determined step) changes with temperature.

Keywords Microkinetic simulation · Cyclohexene dehydrogenation · Turnover frequency · Pt-Cu bimetallic catalyst

Introduction

Cyclohexene is a raw material in organic synthesis, and it could be used as solvent, extractant, and stabilizer. The dehydrogenation of cyclohexene to benzene on the single crystal Pt surface is a typical catalytic reforming process, which has been investigated by various surface science methods [1–5]. A sequential dehydrogenation mechanism [1] was suggested. The π-allyl c-C_6H_9 [1–3] and cyclohexadiene [1, 2] were found as meta-stable intermediates. The Pt was so active that the carbons were produced by 800 K [5], which deactivated the Pt catalyst. Recently, an experiment found that TiO_2-supported Pt could suppress carbon formation during methylcyclohexane dehydrogenation to toluene [6].

High price and the limited supply restrict the application of the pure Pt catalysts. The other components are usually added for the purpose of cutting down the amount of the Pt. Pt-contained bimetallic catalysts have shown extraordinary activity [7–9] and/or selectivity [10, 11]. It is meaningful to explore origins of the special properties of Pt-based bimetallic catalysts. In fact, a great deal of research has been carried out [12–18], and the changed surface electronic properties are responsible for different activities. Besides, it is notable that nickel-based bimetallic catalysts exhibit high sensitivity in dehydrogenation of methylcyclohexane (MCH) to toluene

Electronic supplementary material The online version of this article (https://doi.org/10.1007/s00894-020-04363-y) contains supplementary material, which is available to authorized users.

✉ Shou Chun Feng
1044787664@qq.com

Hong Yan Ma
mahongyan@mail.nankai.edu.cn

Peng Peng Hao
haopeggy@tju.edu.cn

[1] Tianjin University, RenAi College, Tianjin 301636, People's Republic of China

[19–21], and the reason is the addition of Cu or Zn improves the selectivity by occupying the unselective step sites [19, 20].

The Pt/Cu/Pt (111) sandwich structure has drawn our attention. A cyclohexene hydrogenation pathway appeared at 180 K on Pt/Cu/Pt (111) [18]. The corresponding hydrogenation mechanism and the reason for the high hydrogenation activity have been studied in previous work [14]. On the other hand, the Pt/Cu/Pt (111) has also been reported active in catalyzing cyclohexene dehydrogenation at low temperature (179 K and 303 K) [18]. It should be pointed out that the Ni-Zn catalyst has a high selectivity for cyclohexene to benzene at 573.15 K, due to the covered corner and edge sites by Zn [20].

We are curious about the high activity of the Pt/Cu/Pt (111) in both dehydrogenation and hydrogenation at low temperature. In the present paper, the cyclohexene dehydrogenation on the Cu/Pt (111), Pt/Cu/Pt (111), and Pt_4Cu_5/Pt (111) has been investigated based on DFT and microkinetic model analysis. Cu/Pt (111) and Pt_4Cu_5/Pt (111) are also included. At first, both Cu/Pt (111) and Pt/Cu/Pt (111) structures were prepared by depositing Cu on a Pt (111) substrate. At 300 K, Cu/Pt (111) was the main form, but at 600 K, Pt/Cu/Pt (111) was the main production, owing to the migration of surface Cu to the subsurface layer at high temperature [18]. Secondly, the Pt-Cu surface alloy exists in a meta-stable state [22, 23], although it has been proved Pt-Cu surface alloy is thermodynamically less stable than Pt/Cu/Pt(111) according to the surface segregation energy [14]. The Pt concentration on the topmost layer is reckoned as 0.5 in the Cu/Pt (111) structure [22]. So, the model of Pt_4Cu_5/Pt (111) has been built to present the Pt-Cu surface alloy. Since Cu/Pt (111) and Pt_4Cu_5/Pt(111) may exist under the real condition, their catalytic activities are worth of inquiring into.

The aim of this paper is to compare the dehydrogenation pathways of cyclohexene on the Cu/Pt (111), Pt/Cu/Pt (111), and Pt_4Cu_5/Pt (111), and find the factors determining the activity, supplying a possible way to adjust the dehydrogenation activity of the Pt-based bimetallic catalysts. At first, the optimized adsorption structures are present, because the adsorption is the fundamental process for catalytic reactions. Secondly, the transitional states (TSs) is searched and the calculated activation energies are compared with the results in the literature. What is more, the microkinetic model are applied to understand the effect of the desorption barrier, temperature, and the elementary steps on the overall dehydrogenation rate.

Methods and models

The calculations were conducted by the Vienna Ab Initio Simulation Package (VASP) [24, 25]. The exchange–correlation energy and electronic interaction were depicted by the generalized gradient approximation (Perdew–Wang, [26]) and the projector-augment wave scheme [27, 28]. The energy cut off of 400 eV and 3 × 3 × 1 Monkhorst–Pack grid [29] were used for major calculations. A p (3 × 3) unit cell was applied to model the bimetallic surfaces with a vacuum region about 15 Å (Fig. S 1). The spin polarization and dipole correction were involved. A 15 × 15 × 15 $Å^3$ cubic unit cell and a 1 × 1 × 1 Monkhorst–Pack grid have been employed to model gas phase molecules. The Gaussian smearing method with an extending [30] of 0.1 eV was carried out for ionic relaxations calculation. The atoms on the topmost layer of the Cu/Pt (111) and the Pt/Cu/Pt (111) were Cu and Pt, respectively. The surface and subsurface layers as well as the adsorbed molecules were allowed to relax until the forces were within 0.03 eV/Å, and the other layers were fixed. As a result of the shrink or dilation of lattice of the bimetallic surface [31], the optimized Pt–Pt interval of 2.82 Å was wielded on the Pt-based bimetallic surfaces.

The adsorption energy is defined as: $E_{ads,M} = E_{M/surface} - E_{surface} - E_M$. Van der Waals (vdW) interaction could improve the accuracy of the adsorption energy [32, 33]. A systematic increase in the adsorption energies of laterally p-bound unsaturated hydrocarbons (cyclohexene, benzene) was found with the inclusion of vdW interactions [34–37]. The adsorption energy of benzene on Pt (111) corrected by optPBE-vdW [38, 39] matches well with the experiments. The calculated adsorption energy is − 1.62 eV using a six-layer slab model and 7 × 7 × 1 Monkhorst–Pack grid, in good agreement with − 1.66 eV that is obtained by single crystal adsorption calorimetry [40]. As a result, the optPBE-vdW functional is applied for weak mental-molecule interaction systems in our paper, including the adsorption of cyclohexene, 1,3-cyclohexadiene, and benzene.

The TSs were found by the nudged elastic band (NEB) [41] with serial four images along certain elementary step. A quasi-Newton algorithm was chosen to refine the probable TSs though decreasing forces less than 0.05 eV/Å. Finally, the TSs were verified by the presence of the only one normal mode integrated with a pure imaginary frequency. The activation energy (E_a) is the energy dissimilitude between the initial state (IS) and the TS: $E_a = E_{TS} - E_{IS}$. The reaction energy (ΔE) is the energy difference between the IS and the final state (FS): $\Delta E = E_{FS} - E_{IS}$. The zero-point energy correction was also included. The vdW correction was not considered, for its influence on the barriers was negligible as a striking contrast with that on the adsorption energy [14, 36].

Results and discussion

The adsorption of cyclohexene and the dehydrogenation intermediates on the Cu/Pt (111), Pt/Cu/Pt (111), and Pt_4Cu_5/Pt (111) have been investigated at first. The configurations of the most stable adsorption mode are demonstrated in Fig. S 2 and the corresponding energetic data are shown in Table 1.

Table 1 Contributions of each term to the adsorption energies on the Pt/Cu/Pt (111), Cu/Pt (111), and Pt_4Cu_5/Pt (111) surfaces (unit: eV)

Metal surface	Species	E_{ads}	$E_{dis(mole)}$	$E_{dis(sub)}$	E_{int}
Cu/Pt(111)	C_6H_{10}	− 0.91	0.40	0.16	− 1.47
	C_6H_9	− 1.43	0.88	0.48	− 2.79
	C_6H_8	− 1.04	0.95	0.22	− 2.21
	C_6H_7	− 1.73	0.78	0.40	− 2.91
	C_6H_6	− 0.89	0.04	0.08	− 1.01
	C_6H_5	− 2.81	0.45	0.33	− 3.59
Pt/Cu/Pt(111)	C_6H_{10}	− 0.91	0.31	0.06	− 1.28
	C_6H_9	− 1.25	0.85	0.45	− 2.55
	C_6H_8	− 1.33	2.89	0.32	− 4.54
	C_6H_7	− 1.60	0.82	0.38	− 2.80
	C_6H_6	− 1.08	0.01	0.05	− 1.14
	C_6H_5	− 2.66	0.14	0.40	− 3.20
Pt_4Cu_5/Pt(111)	C_6H_{10}	− 1.43	1.91	0.60	− 3.94
	C_6H_9	− 2.82	0.91	0.73	− 4.46
	C_6H_8	− 2.25	1.01	0.95	− 4.21
	C_6H_7	− 2.66	1.17	0.83	− 4.66
	C_6H_6	− 1.97	0.77	0.76	− 3.50
	C_6H_5	− 3.07	0.46	0.61	− 4.14

Adsorption of cyclohexene, π-allyl c-C_6H_9, 1,3-cyclohexadiene, cyclohexadienyl, benzene, and phenyl

The cyclohexene and benzene are physically adsorbed on the Pt/Cu/Pt (111) and Cu/Pt (111) surfaces. The corresponding adsorption energy is in the range of − 0.89~− 1.08 eV. The adsorption height that is the average distance between the olefinic carbons and the surface layer is 2.40~3.20 Å, this is too long to form C-Pt or C-Cu bond. However, on the Pt_4Cu_5/Pt (111), two and four C-Pt bonds are formed when the cyclohexene and benzene are adsorbed (see Fig. S 2). And the corresponding adsorption energies are larger than on the Pt/Cu/Pt (111) or Cu/Pt (111) by at least 0.5 eV.

When two carbons bond with the same metal atom, it is called π interaction. And when one carbon atom only bonds with one metal atom, it is named σ interaction. Three olefinic carbons are in the molecule of π-allyl c-C_6H_9. The most favored configuration is 2σ when the π-allyl c-C_6H_9 is adsorbed on the Pt/Cu/Pt (111), Cu/Pt (111), and Pt_4Cu_5/Pt (111) surfaces (see Fig. S 2). The "chair-like" configuration is preferred by the molecule of 1,3-cyclohexadiene. The σ, 2σ, and 2π adsorption modes are favored on the Cu/Pt (111), Pt/Cu/Pt (111), and Pt_4Cu_5/Pt (111) surfaces, respectively. And the corresponding adsorption energy is − 1.04, − 1.33, and − 2.25 eV, respectively.

The adsorption energy seems have little relationship with the C-Pt or C-Cu bond numbers. Only one or two C-Pt or C-Cu bonds are found in the favored phenyl adsorption mode, whereas four C-Pt or C-Cu bonds are found in the stable cyclohexadienyl adsorption mode. The adsorption energy of phenyl is in the range of −2.66~− 3.07 eV, larger than that of cyclohexadienyl by 0.2~0.9 eV. Different from other species we studied here, phenyl almost stands on the Pt/Cu/Pt (111) surfaces. On the Cu/Pt (111) and Pt_4Cu_5/Pt (111) surfaces, the dihedral angle between the C_6 ring in the phenyl molecule and the surface layer is about 30° (see Fig. S 2). For the same adsorbate, the adsorption energy trend is Pt_4Cu_5/Pt (111) > Cu/Pt (111) ≈ Pt/Cu/Pt (111). Similar adsorption energies of the above species on the Cu/Pt (111) and the Pt/Cu/Pt (111) are attributed to the analogy in the projected densities of states (PDOS) on the *d* orbitals [14].

Decomposition of adsorption energies

By analyzing the terms of the adsorption energy decomposition, a deeper understanding of the adsorption could be achieved. The deformation energy of the molecule ($E_{dis(mole)}$) or the surface ($E_{dis(sub)}$) is defined as the energy difference of the molecule or clean surface in gas phase and in the adsorption mode. The more positive the deformation energies are, the more seriously the molecule or surface deforms during adsorption. What is more, the $E_{dis(mole)}$ is closely related to the energy gap between the highest occupied molecule orbit (HOMO) and the lowest unoccupied molecule orbit (LUMO) [42]. Figure 1 shows the projected density of state of the p_z orbit for each C atom in the molecule of cyclohexene in the gas phase and in the most stable adsorption mode on three surfaces. Two peaks of density of state that are the most close to the Fermi level stand for the HOMO and LUMO. The energy gap is 5.36 eV in the gas phase and 5.23, 5.24, and 1.82 eV on the Cu/Pt (111), Pt/Cu/Pt (111), and Pt_4Cu_5/Pt (111) respectively. The corresponding $E_{dis(mole)}$ is 0.40, 0.31, and 1.91 eV on the Cu/Pt (111), Pt/Cu/Pt (111), and Pt_4Cu_5/Pt (111) respectively, showing the larger $E_{dis(mole)}$ followed by smaller energy gap [14].

The interaction energy (E_{int}) between the adsorbate and the surface is calculated as follows: $E_{int} = E_{ads} - E_{dis(mole)} - E_{dis(sub)}$. Generally speaking, a positive correlation is found between the E_{ads} and the E_{int}. For example, the absolute value of E_{int} and E_{ads} are in the order of $C_6H_5 > C_6H_7 > C_6H_9$ on both the Cu/Pt (111) and Pt/Cu/Pt (111) surfaces. But there are also exceptions, especially on the condition that the deformation energy of the molecule takes the dominant role. For example, large $E_{dis(mole)}$ of 1,3-cyclohexadiene (2.89 eV) leads to large E_{int} (− 4.54 eV) on Pt/Cu/Pt (111).

Dehydrogenation of cyclohexene to benzene

The possible dehydrogenation pathways of cyclohexene on the Cu/Pt (111), Pt/Cu/Pt (111), and Pt_4Cu_5/Pt (111) were investigated on the assumption that hydrogen atoms once produced associate to hydrogen immediately. The structures of

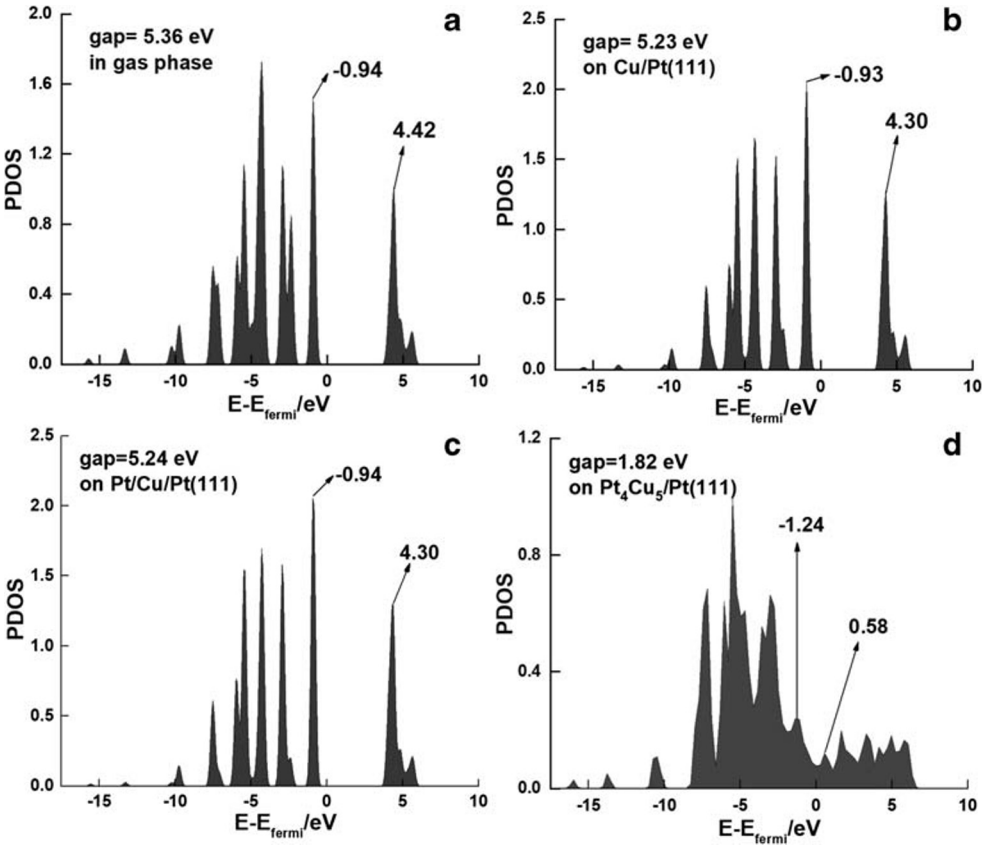

Fig. 1 The projected density of state (PDOS) on the p_z orbital of the C_6H_{10} in the gas phase (**a**) and adsorbed on the Cu/Pt (111) (**b**), Pt/Cu/Pt (111) (**c**), and Pt_4Cu_5/Pt (111) (**d**) surfaces

ISs, TSs, and the calculated activation energies are demonstrated in Fig. 2. The second C-H scission ($C_6H_9 \rightarrow C_6H_8$) is the pivotal dehydrogenation step on the Cu/Pt (111) and Pt/Cu/Pt (111). But on the Pt_4Cu_5/Pt (111), the forth C-H ($C_6H_7 \rightarrow C_6H_6$) scission is key step. The activation energies for the key steps are 0.85, 0.87, and 1.17 eV on the Cu/Pt (111), Pt/Cu/Pt (111), and Pt_4Cu_5/Pt (111), respectively.

The selectivity for gas phase benzene (ΔE) could be estimated as the difference between the barrier of $C_6H_6 \rightarrow C_6H_5$ and the desorption barrier of benzene. The desorption barrier is estimated as $E_{\text{desorption}} \approx \left| E_{\text{ads}} \right| - T\Delta S$. The entropy contributions should be taken into account when the adsorption occurs. About 1/3 transitional entropy is lost after adsorption. The entropy contributions can be calculated according to the

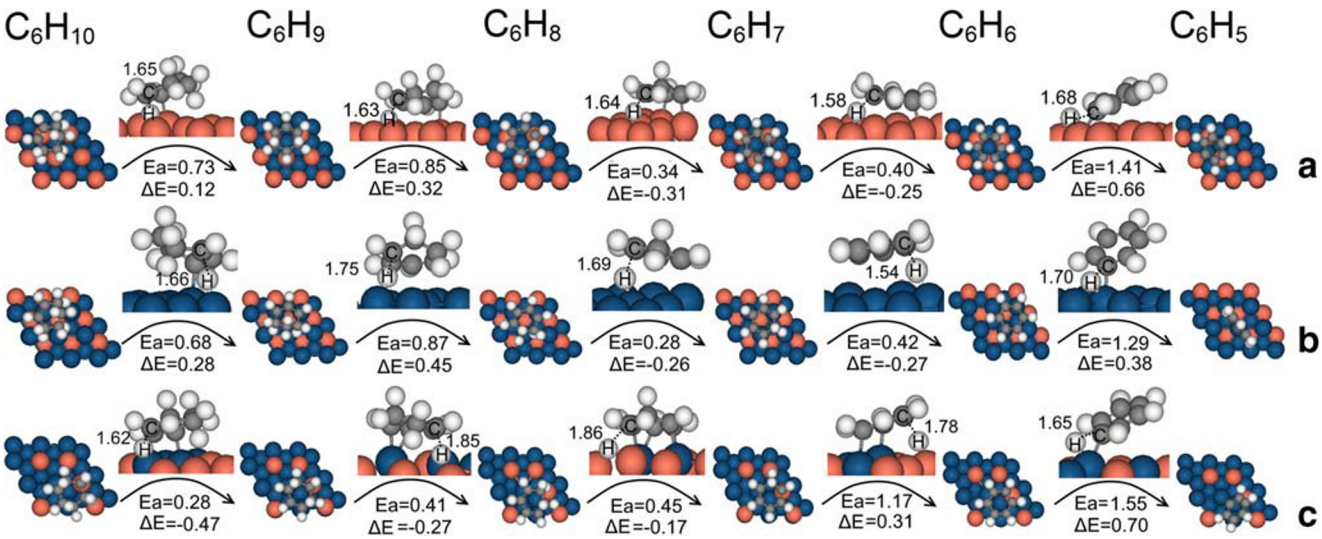

Fig. 2 Possible pathways of cyclohexene dehydrogenation to phenyl on the Cu/Pt (111) (**a**), Pt/Cu/Pt (111) (**b**), Pt_4Cu_5/Pt(111) (**c**). (The unit of E_a and ΔE is eV, the unit of the C-H distance in TS is Å)

Campbell−Sellers equation [43] that is usually used for weakly bound molecular adsorbates:

$$S^0_{ad(T)} = 0.7S^0_{gas(T)} - 3.3R \quad (1)$$

where S^0_{gas} and S^0_{ad} refer to the standard entropy in gas phase and in the adsorption state, respectively. S^0_{gas} can be obtained from the thermochemical data [44]. Under the experimental condition [18] (300 K and 10^{-3} Pa), the contributions of the entropy to the benzene are 0.50 eV. The desorption barriers of benzene are 0.39, 0.58, and 1.47 eV on the Cu/Pt (111), Pt/Cu/Pt (111), and Pt_4Cu_5/Pt (111), respectively. ΔE is in the order of Cu/Pt (111) (1.02 eV) > Pt/Cu/Pt(111) (0.71 eV) > Pt_4Cu_5/Pt (111) (0.08 eV), indicating the selectivity for gas phase benzene on Cu/Pt (111) or Pt/Cu/Pt (111) is much higher than Pt_4Cu_5/Pt (111).

Considering the possible effect of co-adsorbed hydrogen atoms, blocking active sites and moving reaction toward hydrogenation, we studied the influence of H on benzene desorption and dehydrogenation (see table S 1). At first, the adsorption strength of benzene decreases with the increase of H coverage, especially on Pt_4Cu_5/Pt (111) where the adsorption energy of benzene is reduced by 1.2 eV at 4/9 H coverage compared with on clean surface. Secondly, on Cu/Pt (111) and Pt/Cu/Pt (111), the barrier of step ($C_6H_6 \rightarrow C_6H_5$) becomes larger when the concentration of surface H is increased, meaning it becomes difficult for benzene dehydrogenation on H co-adsorbed surface. But a different trend is found on the Pt_4Cu_5/Pt (111): the barrier of step ($C_6H_6 \rightarrow C_6H_5$) decreases with increasing H coverage. This is probably attributed to the obvious destabilized benzene by neighboring H.

According to the above analysis, the co-adsorbed H improves selectivity for gas phase benzene on Cu/Pt (111) and Pt/Cu/Pt (111). However, on Pt_4Cu_5/Pt (111) whether the selectivity could be increased or not depends on H surface coverage, because the nearby H reduces barriers of both benzene desorption and dehydrogenation. For instance, ΔE is 0.07 eV at 1/9 H coverage and 0.85 eV at 4/9 H coverage, suggesting high H concentration prefers benzene desorption. What is more, the co-adsorbed hydrogen obstructs cyclohexene converted to benzene on Cu/Pt (111), Pt/Cu/Pt (111), and Pt_4Cu_5/Pt (111), on the basis of the higher barrier of key step when surface H exists (see Table S 1).

2It should be pointed out that there are several configurations for Pt_4Cu_5/Pt (111). An experiment has found that three adjacent Pt atoms (Pt_3Sn/Pt (111)) are more reactive than two adjacent Pt atoms (Pt_2Sn/Pt (111)) in acetylene hydrogenation [45]. According to the number of neighboring Pt atoms, we build three models for Pt_4Cu_5/Pt (111): two-Pt, three-Pt, and four-Pt neighboring (see Table S 1). By calculating the barrier of $C_6H_7 \rightarrow C_6H_6$ (probable the key step), the barrier of $C_6H_6 \rightarrow C_6H_5$ and the adsorption energy of benzene, we find the barrier on four-Pt neighboring is lower than others, but the selectivity for benzene is poor. Moderate activity and selectivity shown on three-Pt neighboring configuration make it suitable for catalyzing cyclohexene to benzene, and thus this configuration is chosen to represent Pt_4Cu_5/Pt (111).

Microkinetic modeling based on the DFT energetic

To have a deep understanding on the mechanism of cyclohexene dehydrogenation, the microkinetic simulation on the basis of the transition state was carried out. The turnover frequency (TOF (molecules·s^{-1}·$site^{-1}$)) of the elementary step; the surface concentration of the species; and the effect of the adsorption strength, temperature, and pressure on the TOF could be investigated by the microkinetic modeling method [46–48]. The Pt/Cu/Pt (111) is chosen for the microkinetic analysis due to its stability at high temperature, reactivity, and high selectivity for benzene in gas phase. The elementary reaction steps and the corresponding kinetic parameters are listed in Table S 2. The equations used for calculating the rate constant and pre-exponential factor are also shown in Supporting Information. It should be mentioned that the amount of surface hydrogen produced by cyclohexene dehydrogenation could be neglected in the light of low pressure of cyclohexene (10^{-3} Pa) in the experiments [18]. Consequently, the energetic data (adsorption energies and barriers) without hydrogen as spectator is applied in microkinetic simulation.

Desorption barrier of cyclohexene dependence

To understand the effect of the binding strength between cyclohexene and the surface on the individual pathway and overall TOF of $C_6H_{6(g)}$ under the experimental condition (10^{-3} Pa and 300 K) [18], we change the desorption barrier of cyclohexene, meanwhile the other reaction energies and activation barriers remain constant. Figure 3 a shows the volcano-like relationship between the TOF of $C_6H_{6(g)}$ and the desorption barrier of cyclohexene. The up-limit of the TOF of $C_6H_{6(g)}$ is 10^{-4} molecules·s^{-1}·$site^{-1}$ on the Pt/Cu/Pt (111) surfaces. The discrepancy between the highest and lowest TOFs is about 6 orders of magnitude. Besides, with the increasing of the desorption barrier, the surface coverage of $C_6H_{10}^*$ goes up rapidly and reaches monolayer eventually (see Fig. S 3 a). The full monolayer of $C_6H_{10}^*$ should be responsible for the low TOF.

Since the desorption barrier of cyclohexene impacts the TOF of $C_6H_{6(g)}$ greatly, it is important to confirm a proper value of desorption barrier. Based on the discussion about entropy effect, the contribution of the entropy to the cyclohexene is 0.20 eV, and thus the desorption barrier of cyclohexene is 0.71 eV on the Pt/Cu/Pt (111). And the corresponding TOF of $C_6H_{6(g)}$ is 6.4×10^{-5} molecules s^{-1}·$site^{-1}$, close to the up-limit shown in Fig. S 3 a.

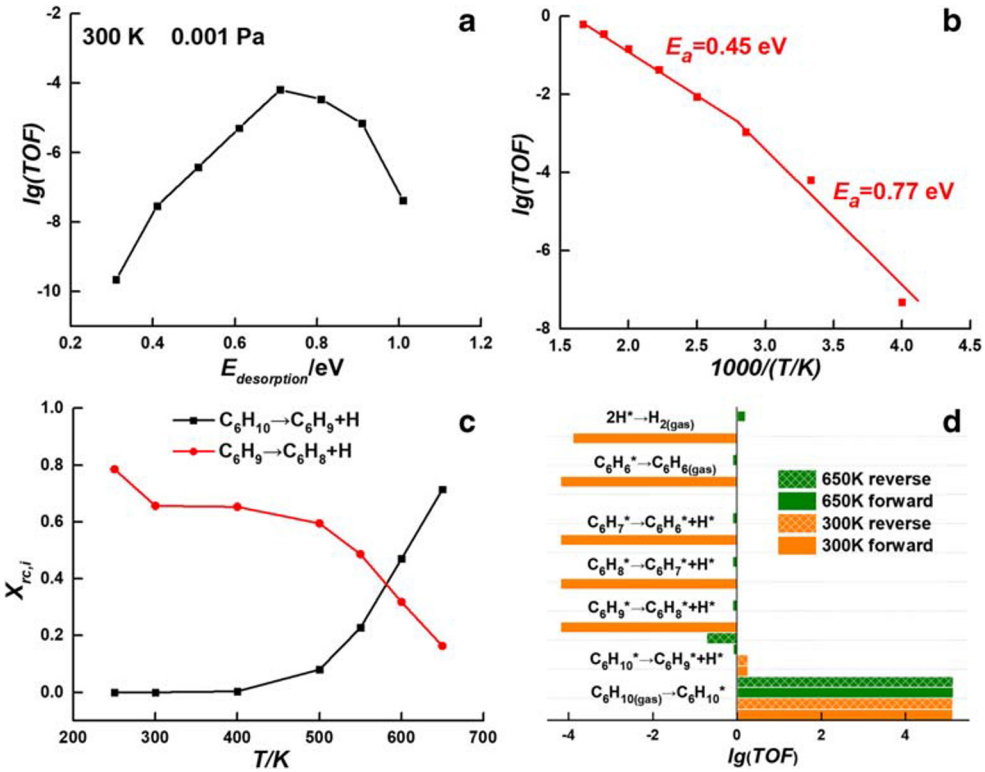

Fig. 3 Relationship between TOF of $C_6H_{6(g)}$ and the desorption barrier of C_6H_{10} (**a**); Arrhenius plot of the TOF of $C_6H_{6(g)}$ (**b**); effect of temperature on $X_{rc,i}$ (**c**); TOF of the main elementary processes at 300 K and 400 K under the 10^{-3} Pa (**d**)

Temperature dependence

The Arrhenius relationship between the TOF of $C_6H_{6(g)}$ and the temperature is shown in Fig. 3b. Between 350 and 650 K, the apparent activation is 0.45 eV, but it is 0.77 eV in the temperature range of 250~350 K. The changes in the slop of the Arrhenius plots indicate the rate-determining step may change with the temperature. In fact, the RDS could be affected by the reverse processes and temperature. The Campbell's degree of rate control [49] ($X_{rc,i}$) is utilized to measure the effect of each dehydrogenation step on the TOF of gas phase benzene. $X_{rc,i}$ is computed on the basis of the equation below:

$$X_{rc,i} = \frac{A_i}{R}\frac{\delta R}{\delta A_i} \tag{2}$$

where R stands for formation rate of gas phase benzene and A_i is the pre-exponential. Ten percent of A_i is altered in both forward and reverse reactions.

As shown in Fig. 3c, between 250 and 500 K $C_6H_9 \rightarrow C_6H_8$ takes dominant role on the TOF of $C_6H_{6(g)}$. At 300 K, the TOF of $C_6H_9 \rightarrow C_6H_8$ is 6×10^{-5} molecules·s^{-1}·$site^{-1}$, and the TOFs of subsequent reactions are almost the same except the TOF of $2H \rightarrow H_{2(gas)}$ (10^{-4} molecules·s^{-1}·$site^{-1}$) (see Fig 3d), indicating $C_6H_9 \rightarrow C_6H_8$ is the RDS. From 500 to 650 K, $X_{rc,i}$ of $C_6H_{10} \rightarrow C_6H_9$ increases quickly with temperature, and $C_6H_{10} \rightarrow C_6H_9$ eventually becomes the RDS above 600 K. In fact, the coverage of free sites is about 0.95 between 300 and 650 K (see Fig S 3 b). This is consistent with our speculation that no surface hydrogen atoms accumulated during cyclohexene dehydrogenation.

Conclusions

We have studied the adsorption of the species involved in cyclohexene dehydrogenated to benzene and the dehydrogenation pathways on the Cu/Pt (111), Pt/Cu/Pt (111), and Pt_4Cu_5/Pt (111) using periodic DFT calculations. The adsorption energies are basically in the sequence: Pt_4Cu_5/Pt (111) > Cu/Pt (111) ≈ Pt/Cu/Pt (111). The low benzene desorption barrier and high barrier of benzene dehydrogenated to phenly on the Pt/Cu/Pt (111) surfaces lead to high selectivity for gas phase benzene. According to the microkinetic model analysis, a volcano relationship between the desorption energy of cyclohexene and the TOF of gas benzene has been found, implying the moderate adsorption strength is favorable for dehydrogenation.

Funding information This project was supported by supported by Tianjin Training Program of Innovation and Entrepreneurship for Undergraduates (201814038022), and Tianjin Municipal Education Commission (2019KJ149, 2018KJ265), China.

References

1. Koel BE, Blank DA, Carter EA (1998) Thermochemistry of the selective dehydrogenation of cyclohexane to benzene on Pt surfaces. J Mol Catal A-Chem 131(1–3):39–53
2. Henn FC, Diaz AL, Bussell ME, Hugenschmidt MB, Domagala ME, Campbell CT (1992) Decomposition of cyclohexene on Pt(111): a BPTDS and HREELS study. J Phys Chem 96(14): 5965–5974
3. Lytken O, Lew W, Harris JJW, Vestergaard EK, Gottfried JM, Campbell CT (2008) Energetics of cyclohexene adsorption and reaction on Pt (111) by low-temperature microcalorimetry. J Am Chem Soc 130(31):10247–10257
4. Pettiette-Hall CL, Land DP, Mclver Jr RT, Hemminger JC (1991) Identification of multiple steps in the dehydrogenation of cyclic C_6 hydrocarbons to benzene on platinum (111). J Am Chem Soc 113(7):2755–2756
5. Rodriguez JA, Campbell CT (1989) Cyclohexene adsorption and reactions on clean and bismuth-covered Pt (111). J Catal 115(2): 500–520
6. Kosaka M, Higo T, Ogo S, Seo JG, Kado S, Imagawa K, Sekine Y (2020) Low-temperature selective dehydrogenation of methylcyclohexane by surface protonics over Pt/anatase-TiO2 catalyst. Int J Hydrogen Energ 45:738–743
7. Ro I, Aragao IB, Chada JP, Liu Y, Rivera-Dones KR, Ball MR, Zanchet D, Dumesic JA, Huber GW (2018) The role of Pt-Fe_xO_y interfacial sites for CO oxidation. J Catal 358:19–26
8. Kang Y, Bu X, Wang G, Wang X, Li Q, Feng Y (2016) A highly active Cu–Pt/SiO_2 bimetal for the hydrogenolysis of glycerol to 1, 2-Propanediol. Catal Lett 146(8):1408–1414
9. Singh JA, Yang N, Liu X, Tsai C, Stone KH, Johnson B, Koh AL, Bent SF (2018) Understanding the active sites of CO hydrogenation on Pt-Co catalysts prepared using atomic layer deposition. J Phys Chem C 122(4):2184–2194
10. Marcinkowski MD, Darby MT, Liu J, Wimble JM, Lucci FR, Lee S, Michaelides A, Flytzani-Stephanopoulos M, Stamatakis M, Sykes ECH (2018) Pt/Cu single-atom alloys as coke resistant catalysts for efficient C-H activation. Nat Chem 10:325–332
11. Jiang Z, Wan W, Lin Z, Xie J, Chen JG (2017) Understanding the role of M/Pt(111) (M = Fe, Co, Ni, Cu) bimetallic surfaces for selective hydrodeoxygenation of furfural. ACS Catal 7(9):5758–5765
12. Ma HY, Shang ZF, Xu WG, Wang GC (2012) Cyclohexene dehydrogenation to produce benzene on nAu/Pt(100) and nPt/Au(100) (n = 0, 1, 2) surfaces from a first-principles study. J Phys Chem C 116(18):9996–10008
13. Ma HY, Wang GC (2011) Theoretical study of 1,3-cyclohexadiene dehydrogenation on Pt (111), Pt_3Sn/Pt (111), and Pt_2Sn/Pt (111) surfaces. J Catal 281(1):63–75
14. Ma HY, Wang GC (2018) Hydrogenation of cyclohexene on the M/Pt(111) and Pt/M/Pt(111) (M = Fe, Co, Ni, and Cu) surfaces from a systematic DFT study. J Phys Chem C 122(29):16692–16703
15. Wang YF, Li K, Wang GC (2018) Formic acid decomposition on Pt_1/Cu (111) single platinum atom catalyst: insights from DFT calculations and energetic span model analysis. Appl Surf Sci 436(1): 631–638
16. Wang H, Stamatakis M, Hansgen DA, Caratzoulas S, Vlachos DG (2010) Understanding mixing of Ni and Pt in the Ni/Pt(111) bimetallic catalyst via molecular simulation and experiments. J Chem Phys 133(22):224503
17. Corredor EC, Kuhrau S, Kloodt-Twesten F, Frömter R, Oepen HP (2017) SEMPA investigation of the Dzyaloshinskii-Moriya interaction in the single, ideally grown Co/Pt(111) interface. Phys Rev B 96:060410(R)
18. Humbert MP, Chen JG (2008) Correlating hydrogenation activity with binding energies of hydrogen and cyclohexene on M/Pt (111) (M = Fe, Co, Ni, Cu) bimetallic surfaces. J Catal 257(2):297–306
19. Al-ShaikhAli AH, Jedidi A, Cavallo L, Takanabe K (2015) Non-precious bimetallic catalysts for selective dehydrogenation of an organic chemical hydride system. Chem Commun 51:12931–12934
20. Al-ShaikhAli AH, Jedidi A, Anjum DH, Cavallo L, Takanabe K (2017) Kinetics on NiZn bimetallic catalysts for hydrogen evolution via selective dehydrogenation of methylcyclohexane to toluene. ACS Catal 7:1592–1600
21. Patil SP, Pande JV, Biniwale RB (2013) Non-noble Ni-Cu/ACC bimetallic catalyst fordehydrogenation of liquid organic hydrides for hydrogen storage. Int J Hydrogen Energ 38:15233–15241
22. Barrett NT, Belkhou R, Thiele J, Guillot C (1995) A core-level photoemission spectroscopy study of the formation of surface alloy Cu/Pt(111): comparison with Pt/Cu(111). Surf Sci 331-333:776–781
23. Belkhou R, Barrett NT, Guillot C, Fang M, Barbier A, Eugène J, Carrière B, Naumovic D, Osterwalder J (1993) Formation of a surface alloy by annealing of Pt/Cu(111). Surf Sci 297(1):40–56
24. Kresse G, Furthmüller J (1996) Efficiency of ab-initio total energy calculations for metals and semiconductors using a plane-wave basis set. J Comput Mater Sci 6(1):15–50
25. Kresse G, Furthmüller J (1996) Efficient iterative schemes for abinitio total-energy calculations using a plane-wave basis set. Phys Rev B: Condens Matter Mater Phys 54(16):11169–11186
26. Perdew JP, Wang Y (1992) Accurate and simple analytic representation of the electron-gas correlation energy. Phys Rev B: Condens Matter Mater Phys 45(23):13244–13249
27. Kresse G, Joubert D (1999) From ultrasoft pseudopotentials to theprojector augmented-wave method. Phys Rev B: Condens Mater Phys 59(3):1758–1775
28. Blöchl PE (1994) Projector augmented-wave method. Phys Rev B: Condens Matter Mater Phys 50(24):17953–17979
29. Monkhorst HJ, Pack JD (1976) Special points for brillouin-zone integrations. Phys Rev B: Solid State 13(12):5188–5192
30. Elsässer C, Fähnle M, Chan CT, Ho KM (1994) Density- functional energies and forces with Gaussian-broadened fractional occupations. Phys Rev B: Condens Matter Mater Phys 49(19):13975–13978
31. Kitchin JR, Khan NA, Barteau MA, Chen JG, Yakshinskiy B, Madey TE (2003) Elucidation of the active surface and origin of the weak metal-hydrogen bond on Ni/Pt(111) bimetallic surfaces: a surface science and density functional theory study. Surf Sci 544(2–3):295–308
32. Gauthier Y, Schmid M, Padovani S, Lundgren E, Buš V, Kresse G, Redinger J, Varga P (2001) Adsorption sites and ligand effect for CO on an alloy surface: a direct view. Phys Rev Lett 87(3): 036103(4)
33. Gautier S, Steinmann SN, Michel C, Fleurat-Lessarda P, Sautet P (2015) Molecular adsorption at Pt(111). How accurate are DFT functionals? Phys Chem Chem Phys 17:28921–28930
34. Lakshmikanth KG, Ayishabi PK, Chatanathodi R (2017) Ab initio DFT studies of adsorption characteristics of benzene on close-packed surfaces of transition metals. Comput Mater Sci 137:10–19
35. Ayishabi PK, Chatanathodi R (2017) Adsorption of benzene on low index surfaces of platinum in the presence of van der Waals interactions. Surf Sci 664:8–15
36. Trinh QT, Nguyen AV, Huynh DC, Pham TH, Mushrif SH (2016) Mechanistic insights into the catalytic elimination of tar and the promotional effect of boron on it: first-principles study using toluene as a model compound. Catal Sci Technol 6:5871–5883
37. Yildirim H, Greber T, Kara A (2013) Trends in adsorption characteristics of benzene on transition metal surfaces: role of surface

chemistry and van der Waals interactions. J Phys Chem C 117(40): 20572–20583
38. Klimeš J, Bowler DR, Michaelides A (2010) Chemical accuracy for the van der Waals density functional. J Phys Condens Matter 22(2): 022201
39. Klimeš J, Bowler DR, Michaelides A (2011) Van der Waals density functionals applied to solids. Phys Rev B 83(19):195131
40. Carey SJ, Zhao W, Campbell CT (2018) Energetics of adsorbed benzene on Ni(111) and Pt(111) by calorimetry. Surf Sci 676:9–16
41. Mills G, Jónsson H (1994) Quantum and thermal effects in H_2 dissociative adsorption: evaluation of free energy barriers in multidimensional quantum systems. Phys Rev Lett 72(7):1124–1127
42. Morin C, Simon D, Sautet P (2006) Intermediates in the hydrogenation of benzene to cyclohexene on Pt(1 1 1) and Pd(1 1 1): a comparison from DFT calculations. Surf Sci 600(6):1339–1350
43. Campbell CT, Sellers JRV (2012) The entropies of adsorbed molecules. J Am Chem Soc 134(43):18109–18115
44. Barin I (1995) Thermochemical data of pure substances. VCH Verlag, Weinheim, pp 297–298
45. Gao J, Zhao H, Yang X, Koel BE, Podkolzin SG (2014) Geometric requirements for hydrocarbon catalytic sites on platinum surfaces. Angew Chem Int Ed 53(3):641–3644
46. Li MR, Wang GC (2016) Ethanol reaction on Co_3O_4(110) and Co(0001): a microkinetic model analysis. J Phys Chem C 120(49):28110–28124
47. John P, Clay JP, Greeley JP, Ribeiro FH, Delgass WN, Schneider WF (2014) DFT comparison of intrinsic WGS kinetics over Pd and Pt. J Catal 320:106–117
48. Prats H, Gamallo P, Illas F, Sayós R (2016) Comparing the catalytic activity of the water gas shift reaction on Cu (321) and Cu (111) surfaces: step sites do not always enhance the overall reactivity. J Catal 342:75–83
49. Campbell CT (1994) Future directions and industrial perspectives micro- and macro-kinetics: their relationship in heterogeneous catalysis. Top Catal 1:353–366